Phase Contrast Imaging for Wendelstein 7-X

Applicant/Institution:
Massachusetts Institute of Technology
77 Massachusetts Avenue
Cambridge, MA 02139

Principal Investigator
Prof. Miklos Porkolab
Department of Physics
Tel 617-253-8448
porkolab@psfc.mit.edu

Administrative Contact
Jamie Goldberg
Office of Sponsored Programs
Tel 617-253-6287
jrgold@mit.edu

Subaward Applicant/Institution:
SUNY Cortland
PO Box 2000
Cortland, NY 13045

Subaward Investigator
Asst. Prof. Eric Edlund
Department of Physics
Tel 607-753-5697
eric.edlund@cortland.edu

Administrative Contact
Thomas Frank
Office of Research and Sponsored Programs
Tel 607-753-2511
thomas.frank@cortland.edu

Funding Opportunity Announcement Number: DE-FOA-0002429
PAMS Preproposal Number: PRE-0000025077
DOE/Office of Science Program Office: Office of Fusion Energy Sciences
DOE/Office of Science Program Office Technical Contact: Dr. Samuel J. Barish

Contents

Phase Contrast Imaging for Wendelstein 7-X

1 Introduction

The main objective of the work proposed in this application is to continue operation of the phase contrast imaging (PCI) diagnostic that is installed on the Wendelstein 7-X (W7-X) stellarator. This work has been previously funded under two prior grants, first to design and build the diagnostic, and secondly to continue operations, implement design improvements, and conduct data analysis from the OP 1.2b campaign until the present. The PCI diagnostic has been very successful in acquiring measurements of turbulence and other fluctuations. Results from these measurements have been featured in numerous publications [1–7] and presentations [8–30] over the last three years.

Near-term work under this grant would provide funding to complete the re-installation of the PCI diagnostic, which had to be partially disassembled to make room for the water cooling lines for the actively coold divertor modules. Following installation of the diagnostic, commissioning and testing of the integrated system will be conducted. The final phase of this grant will fund operations into the OP2 campaign. Throughout this period, additional data analysis, synthetic diagnostic development, and diagnostic improvements will continue.

1.1 The phase contrast imaging method

Light waves passing through spatial fluctuations in a plasma will scatter at small angles, with a scattering angle proportional to the wavenumber of the plasma waves. Importantly, the plasma appears to the light waves as a phase object, which means that the scattered components are out of phase with the unscattered component by $\pi/2$ for a coherent light source. This difference in phases can be exploited to create an image of the fluctuations by manipulating the relative phase between components. This is accomplished with an an optical device called a "phase plate," which is located at a Fourier plane of the optical system, as illustrated in Fig. 1. By retarding the phase of the unscattered component by $\pi/2$ by forcing it to travel a slighter longer distance, equal to to $\lambda/4$ of the laser wavelength, the unscattered component and scattered components are brought into phase with each other.

The image formed from these components after phase manipulation exhibits a variation in amplitude that is proportional to the line integral of the electron density fluctuations along the beam path. That is, the measured intensity, I, is given by

$$I = C \int \tilde{n}_e dz, \tag{1}$$

where the integral of the electron density fluctuations ($\tilde{n}_e$) is taken along the beam path through the plasma, and C is a constant that depends on the detector characteristics, laser wavelength, and physical constants. The actual measurements are further modified by the detector response, including finite frequency and spatial ranges measurable by the detector, are modified by the phase plate and other optics, and subject to various noise sources. The phase contrast technique is rather insensitive to errors in equilibrium reconstruction, and plasma motion enters into the signal as a simple Doppler shift. Absolute calibration of the density fluctuations measured by PCI is performed by measuring the fluctuations induced by small changes in the index of refraction of air when sound

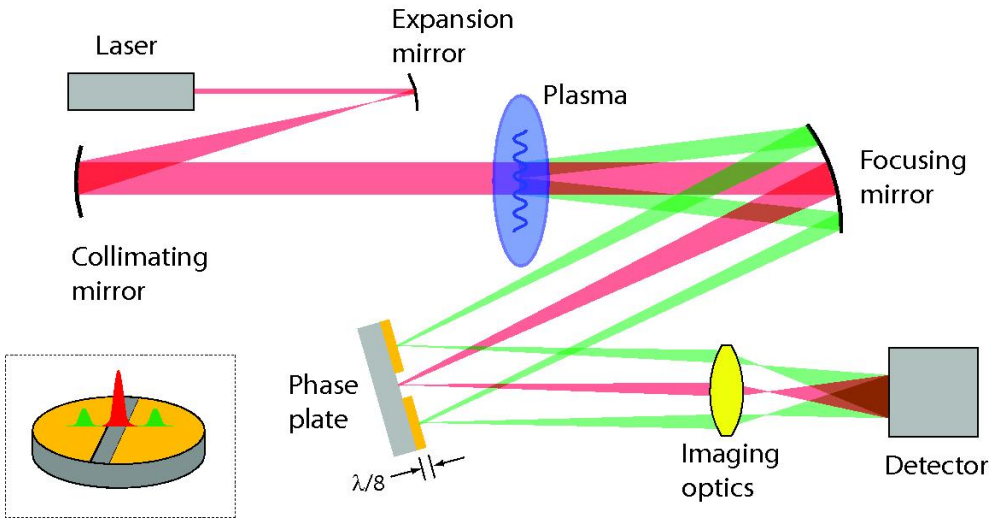

Figure 1: Illustration of the PCI showing the scattering of light from plasma waves, phase manipulation by the phase plate at a Fourier plane of the system, and image reconstruction at the detector.

waves of known intensity are launched across the path of the PCI laser beam on the transmitting table.

The main complication in the measurements is the interpretation of the line-integrated nature of the fluctuations, which naturally leads to a "synthetic diagnostic" approach implemented in codes, and is discussed further in Section 2.2. While the PCI measurements themselves constrain the absolute fluctuation levels, it is possible that phase cancellation effects resulting from summing positive and negative density fluctuations can reduce or enhance the apparent magnitude of the density fluctuations, as is especially present in measurement of MHD modes. However, the spatial structure of the integrated fluctuations is quite sensitive to the 2D structure of the fluctuations and contains enough information that the radial location of coherent modes can be constrained [31].

1.2 The PCI diagnostic at Wendelstein 7-X

The PCI diagnostic was installed on the W7-X stellarator in 2017 and saw first operation in the OP 1.2b campaign [1, 7]. The first two years of operation, through the end of the OP1.2b campaign, included many developments, changes, and refinements in the design.

A number of major changes to the diagnostic installation are being made in preparation for the OP2 campaign. The water cooling lines for the actively cooled divertor require that the transmitting table be relocated from its former location in the second basement level to a new location. The receiving table, however, will remain in the same location as before. These changes have required substantial modification to the beamlines and mirror boxes that redirect the laser beam through the torus.

A set of 12" diameter steering mirrors, mirror mounts, and motors for remote control have been purchased, and most of the hardware for the new installation has been designed and fabricated. Installation for some of the new beam line components has already been completed, with the remainder to be done in the spring and summer of 2021.

The new optics configuration for the transmitting table is complete and initial testing of the setup is being undertaken in one of the laboratory spaces at IPP Greifswald. The major change to the transmitting system is the new laser, a research-grade, high-stability CO_2 laser from Access Laser. Characterization of the laser in terms of stability and beam shape quality are being performed using multiple measurement systems.

Transmitting and receiving optics

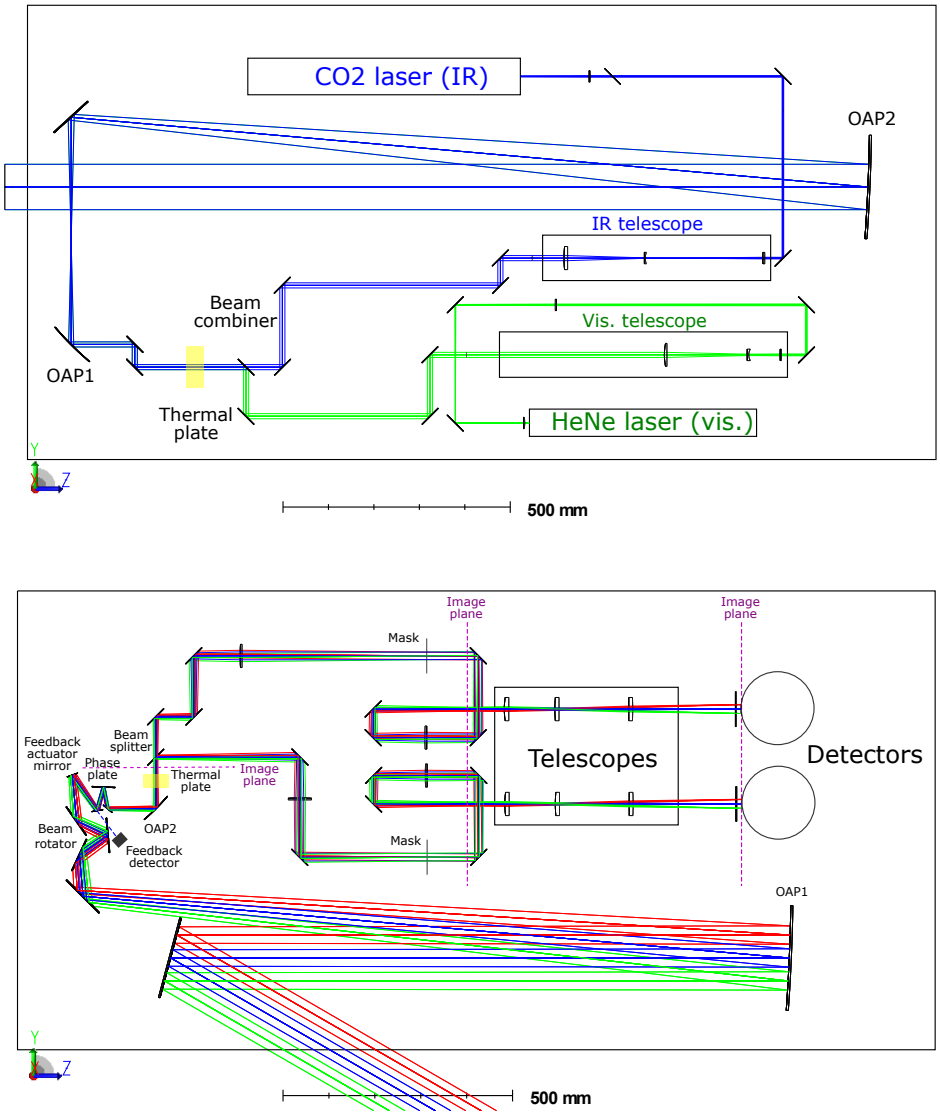

Figure 2: (Top) Optical design of the transmitting table. Blue and green lines represent the IR CO_2 and visible HeNe laser beam paths, respectively. (bottom) Optical design of the receiving table. Different colors represent the scattered rays from the center and two edges of the laser beam.

The laser optical table houses the lasers and prepares the beam for passage through the experiment. Its primary purposes are to magnify the probing infrared (IR) beam to its (variable) final diameter for plasma vessel passage, to remotely co-align the invisible IR beam with an additional visible pilot laser for alignment purposes, and to monitor the incident IR beam power and quality during operation.

The optical design of the laser table as calculated by the program Zemax© can be seen in Fig. 2 (top). The probe laser beam of the PCI system is generated by a continuous wave (CW) 100 W, 10.6 μm infrared CO_2 laser (Synrad Firestar t60) in the first operation campaign in 2017-2018, and is upgraded to a 20 W AL-20SLT Access Laser. A $f = 500$ mm lens is placed 350 mm in front of the laser aperture to reduce the Gaussian beam expansion. The beam then passes two 50% beam splitters and enters a telescope consisting of three ZnSe lenses: one plano-convex 1" diameter $f = 200$ mm lens (Thorlabs), one plano-concave 1" diameter lens $f = -50$ mm lens (Thorlabs), and one plano-convex 2" diameter $f = 200$ mm lens (II-VI Infrared). The magnification range of the telescope is about $M = 0.8$ to 4, resulting in a beam diameter ranging from about 2.8 mm to 15.7 mm after traversing 1500 mm on the optical table before entering the next telescope.

A 12 mW, 632.8 nm HeNe laser, Melles-Griot model, is combined with the IR beam to assist with alignment. The HeNe laser beam first passes through a fixed telescope consisting of a $f = 150$ mm and a $f = 500$ mm lens. An adjustable 3-lens telescope similar to the IR one is also used to expand the HeNe laser beam to the same size as the probe beam: one plano-convex 1" diameter $f = 250$ mm lens, one plano-concave 1" diameter lens $f = -50$ mm lens, and one plano-convex 2" diameter $f = 250$ mm lens. The magnification range is from $M = 0.62$ to 3.62 to match up with the IR beam size. The two laser beams are then combined by a beam combiner.

While not illustrated in Fig. 2, two remote controllable flippable mirrors are installed between the beam combiner and the next optic. They are used to redirect the beam with different optical path lengths onto a thermal UV imaging plate for remote co-alignment checks. The combined beams are then expanded with a telescope comprised of two off-axis parabolic (OAP) mirrors with a fixed magnification of $M = 80"/9" = 8.9$. The final beam size off the laser table can vary from 25 mm to 140 mm, and typically $80 - 100$ mm is used.

The detector optical table houses the phase plate, detectors and associated beam manipulation hardware. Its purposes are: de-magnification of the beam to a manageable size and rotation of the image into the correct reference frame, active feedback control of the beam position, passage through the phase plate for phase contrast generation, beam power monitoring and verification of co-alignment with the pilot laser, selection of probing range along the beam path by geometrical masking, and finally signal detection by the detectors.

Figure 2 (bottom) shows the optical design of the detector table, in which the different colored rays represent the scattered beam from the center and the two edges. The returning laser beam is first mapped onto a large 9" diameter, 80" focal length OAP mirror, which focuses the beam onto the phase plate at its focal plane.

The converging beam is first sent through a beam rotator consisting of three plane mirrors, which ensures that the image of a plasma filament along the poloidal direction is aligned with the horizontal 1d detector array on the detector table. After the beam rotator, a steerable mirror reflects the beam onto a beam splitter which reflects 99% of the IR beam power onto the phase plate. A subsequent quadrature detector is installed behind the beam splitter. Its purpose is to form a feedback vibration compensation system with the steerable mirror to ensure a stable beam position on the phase plate. The reflected component of the beam from the phase plate is collimated

by a 6" OAP mirror, which forms a telescope with a fixed magnification of $M = 6"/80" = 0.075$ with the large OAP mirror.

The phase plate (manufactured by Spire Semiconductor) is essentially a 2" gold plated mirror with a 1.1 mm wide groove crossing the center. The low-k diagnostic limit is then determined by the groove width to be $k_c = \pi d/\lambda f = 1.6$ cm^{-1}, where λ is the wavelength of the IR laser, $f = 80"$ is the focal length of the large OAP, and d is the groove width. The depth of the groove is $\lambda/8 = 1.325$ μm to create a $\pi/2$ phase shift between the unscattered and scattered components. The ZnSe material of the groove has a reflection coefficient of $\rho = 0.28$, which increases the signal intensity by a factor $1/\sqrt{\rho} = 1.89$. A power meter behind the phase plate is used to measure the transmitted power through the phase groove, and of the entire optical system to this point.

A remote controllable flippable mirror is installed between the small OAP mirror and the next optic to redirect the beam to another thermal UV imaging plate for alignment and beam quality checks. The location of the flipping mirror is chosen so that the IR plate is located at the image plane created by the OAP telescope of the plasma in the vacuum vessel. This image plane is otherwise located right in front of the beam splitter without the flippable mirror.

The beam splitter sends the beam down to two separate beam paths. In each path, the laser beam first enters a $M = 1$ telescope with two 2" diameter, 16" focal length ZnSe lenses to create a second focal plane where the radial localization mask is located, then passes through a remotely adjustable telescope which sets the detectable wavenumber range, and finally reaches the detector. The net magnification of the system is then equal to the product of the magnification of the OAP telescope (0.075) and the magnification of the adjustable telescope.

The $M = 1$ telescope creates a second image plane 16" after this telescope, 75 mm before the final adjustable telescope. This image plane acts as a virtual object plane which is imaged by the adjustable telescopes onto the detectors, with a wide range of magnification. The linear stages of the two telescopes are connected so that the magnifications are the same for the two detectors. Both telescopes consist of three plano-convex 2" diameter ZnSe lenses manufactured by Laser Research Optics, with focal lengths $f = 5"$, 8.75" and 16", respectively. The magnification ranges from 1 to 5, which translates to a net magnification $M = 2.67$ to 13.33. This means the Nyquist wavenumber is from $k_N = 4.7$ to 23.5 cm^{-1} with 0.5 mm detector element spacing, which is sufficient to well resolve ion-scale turbulence. In most discharges, the net magnification is set to 5, with the exception of late phase of the campaign, when the net magnification is set to be 3 to extend the wavenumber range for high-k fluctuations. It is worth noting that the magnification of the system is solely dependent on the detector table optics, and independent of the laser beam size.

1.3 An overview of PCI measurements from Wendelstein 7-X

The PCI system on W7-X has been run successfully for two operation campaigns, and in this time has reliably and continuously acquired data for most discharges. It has been a central tool for continuously monitoring density fluctuations and providing feedback on favorable conditions regarding improved confinement at reduced turbulence levels.

Figure 3 (a) shows a frequency spectrogram of density fluctuations measured by a single line-of-sight of the PCI diagnostic. The turbulent spectrum is broadband and its power decays exponentially towards high frequencies. An oscillation of the fluctuation amplitude can be observed, especially in the low frequency range ($f < 300$ kHz), this is mainly due to the oscillation in bulk plasma density as shown in Fig. 3 (b). Here the line-integrated plasma density (blue line) is measured by an interferometer diagnostic. The density fluctuations amplitude is calculated by in-

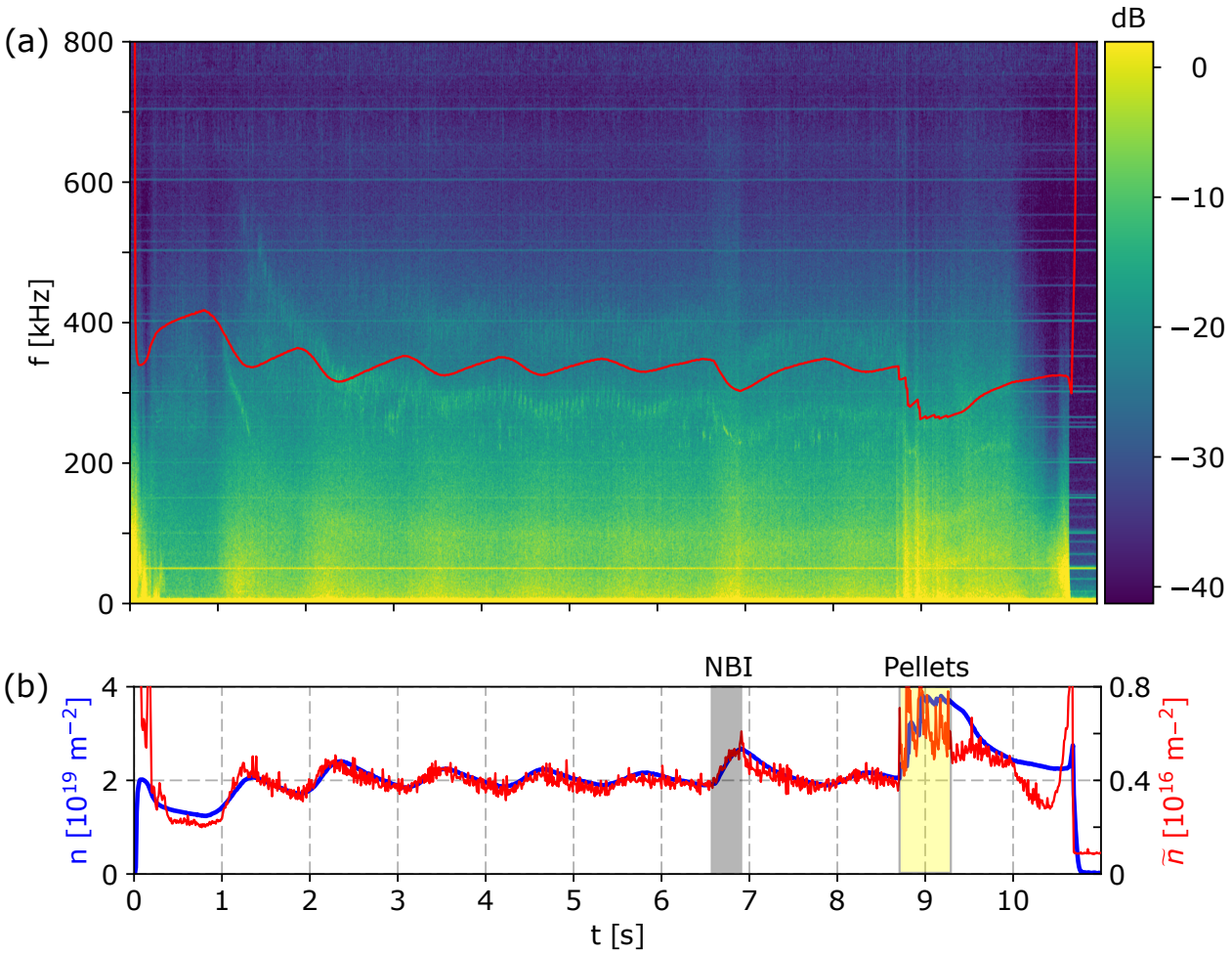

Figure 3: Overview of W7-X program XP20180822.017. Top: Frequency spectrogram of PCI showing the broadband density fluctuations and several coherent mode. The red line indicates the theoretical Alfvén frequency; bottom: line-integrated density and density fluctuations measured by interferometer and PCI, respectively.

tegrating the spectrogram in Fig. 3 (a) over the frequency range $10 - 1000$ kHz. The low frequency component $f < 10$ kHz is omitted to avoid noises from the laser. An additional 3 MW NBI heating from $t = 6.6$ to 6.9 s and a series of cryogenic pellet injections from $t = 8.7$ to 9.3 s both induce changes in the fluctuation spectrum.

The density fluctuation amplitude scales well with the line-integrated density throughout the discharge up to the pellet injection, including the NBI phase. In a transient phase after pellet injection from $t = 9$ to 9.6 s, a drop in the fluctuation amplitude compared to the plasma density can be observed. This temporary reduction of turbulence is believed to be the main reason for the transient boost in confinement post pellets [3].

Alfvénic modes

Coherent modes in the range of several hundreds of kilohertz can also be observed in the spectrum. They are thought to be Alfvénic in nature due to the correlation with the Alfvén frequency that is inversely proportional to the square root of density, indicated by the red line in Fig. 3 (a). It is noted that the theoretical Alfvén frequency is calculated from the line-integrated density, which is not the local plasma density where the Alfvén modes were developed. Therefore, it is only used as an indication of the frequency evolution, but not necessarily fits exactly with the observed mode frequency. These Alfvénic modes were frequently observed by the PCI diagnostic even though most plasma were produced and maintained purely with ECH and thus absent of energetic-ions. This is also suggested by the fact that these modes could only be observed in low density plasmas, typically with line-integrated density below 6×10^{19} m^{-2}. It has been suggested that they are excited by the thermal electron population or energetic trapped electrons [32].

Broadband fluctuations during confinement transitions

Plasma density peaking in W7-X can be achieved both by cryogenic pellet injection or NBI. For the pellet-fueled scenario, Fig. 4, a sequence of pellets is injected into an initial line-averaged density of $n = 3 \times 10^{19}$ m^{-3} between $t_\mathrm{A} = 1.0$ s and $t_\mathrm{B} = 1.7$ s, accompanied by an increase of the heating power. The plasma density increases and reaches its peak value at t_B with $n = 8 \times 10^{19}$ m^{-3} followed by a smooth decrease. During this period, and distinctly after the end of the pellet sequence, the plasma stored energy increases sharply from $W_\mathrm{dia} = 0.3$ MJ to a peak exceeding 1 MJ, a value that is unattainable in gas-fueled discharges at equal densities, thereby indicating strongly improved plasma confinement which lasts until t_D.

Before pellet injection ($t < t_\mathrm{A}$) and after the end of improved confinement ($t < t_\mathrm{D}$), the turbulent fluctuation spectra are broadband and featureless, while their magnitude scales with W_dia. The pellet injection process itself creates large density perturbations that show up as distinct spikes. Between t_B and t_D, fluctuations then decrease markedly, which is especially remarkable since the stored energy is rising simultaneously while the density exhibits only a weak decrease. The signal reaches a minimum at t_C, after which high-frequency fluctuations set in that rapidly decrease in frequency as they increase in magnitude. This rise is accompanied by a decrease in the temporal derivative of W_dia, which finally falls off. Afterwards, density fluctuation levels and spectra return to values in line with results from gas-fueled discharges.

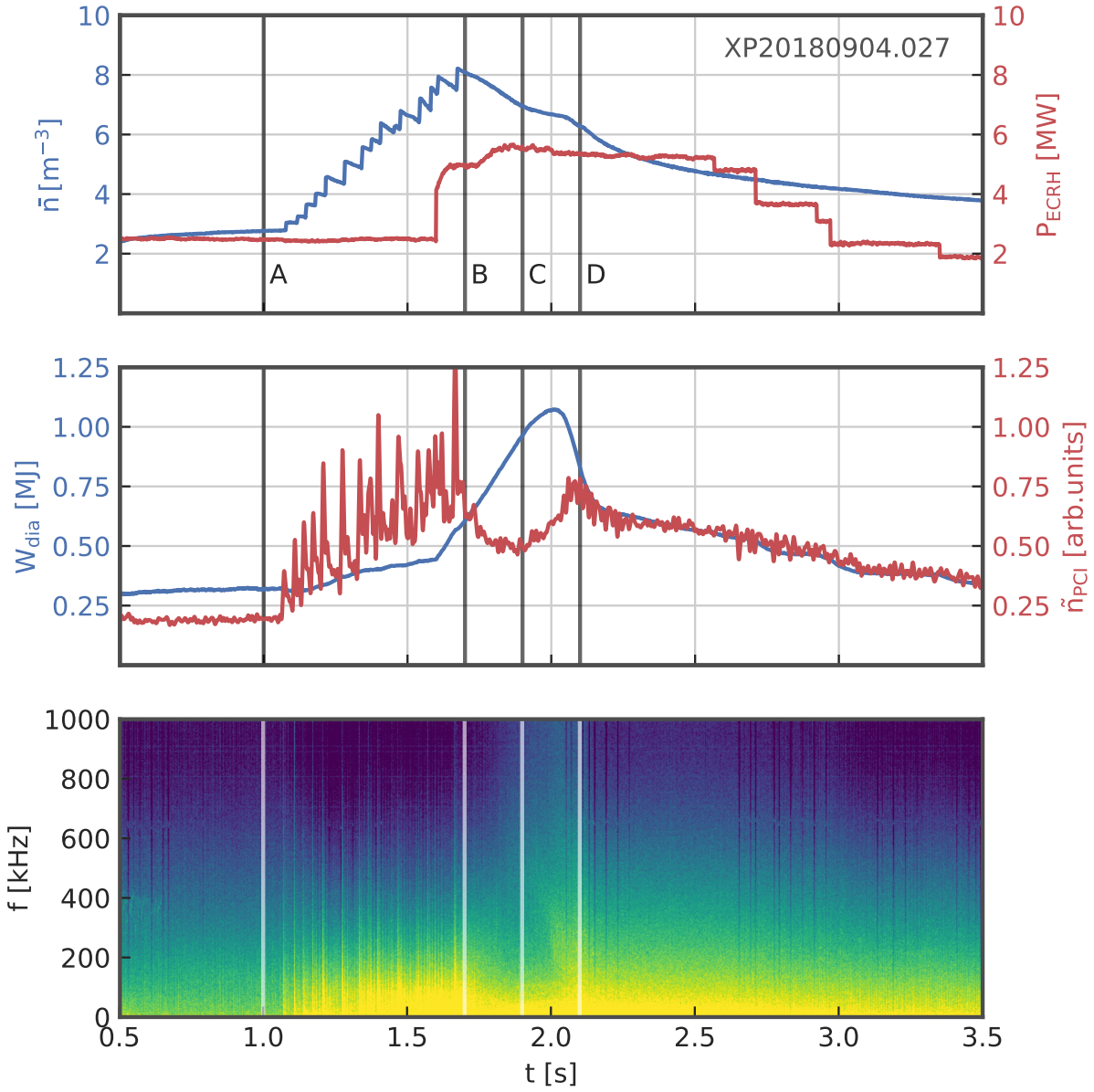

Figure 4: Overview for W7-X program XP20180904.027. Top: line-integrated density and ECH power, center: line-integrated density fluctuations measured by PCI and diamagnetic energy, bottom: spectrogram of PCI fluctuations.

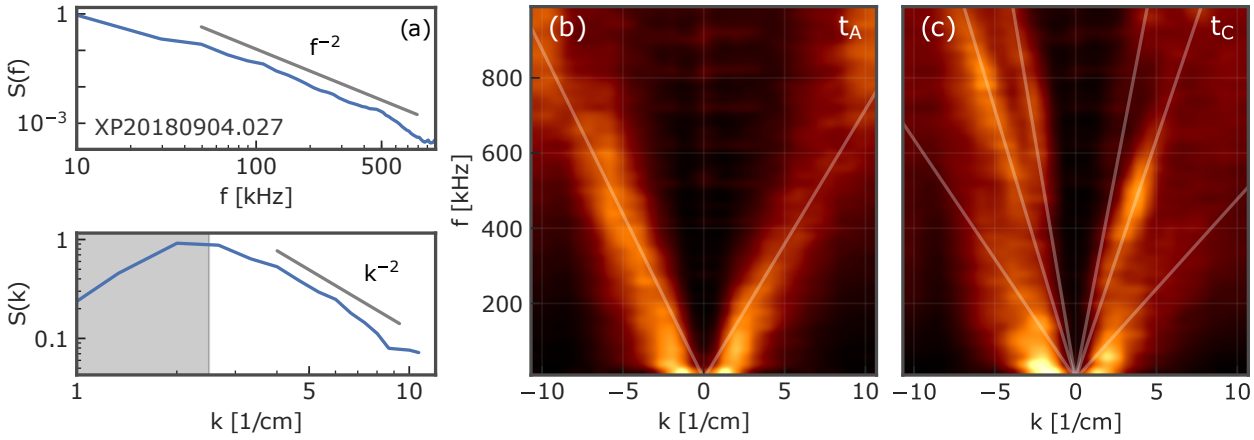

Figure 5: PCI frequency-wavenumber spectra of density fluctuations (a) without normalization at t_A, (b) and (c) frequency-normalized at t_A and t_C, respectively. White lines indicate dominant phase velocities.

Measurement of turbulent phase velocities

Figure 5 (a) shows the unnormalized frequency-wavenumber spectrum $S(k_\perp, f)$ of fluctuation power at poloidal wavenumbers $k_\perp$ and frequencies f at the time point t_A. It shows clear power law behavior in both f-and k-space (when taking the low-k instrument limit at $k_\perp = 1.6$ cm^{-1} into account). The fluctuation power is predominantly at ion scales, with $k_\perp \rho_s = 1$ at $k_\perp \approx 4$ cm^{-1}, depending on the radial position. It is further centered around a constant phase velocity $v_\mathrm{ph} = 2\pi f / k_\perp$ in both positive and negative direction as denoted by white lines, where the sign of k corresponds to an upward or downward propagation in the coordinate system of the experiment. This becomes more apparent when normalizing the k-spectra to unity at each frequency, as done for Figs. 5 (b) and (c). We identify the phase velocities in Fig. 5 (b) as fluctuations propagating with the $E \times B$ drift, where the two branches correspond to the inboard and outboard side. Both sides are regions of bad curvature in which drift-wave instabilities can develop at the toroidal location of PCI in W7-X. The k-f spectra in Fig. 5 (c) at t_C when confinement is improved show remarkable behavior not observed during regular gas-fueled discharges: several distinct and simultaneous phase velocities indicate a qualitative change in turbulence which persists from t_B to shortly before t_D, when a single dominant phase velocity is recovered and the situation is again analogous to that before pellet injection.

1.4 Support of research priorities defined in the FOA

The following summarizes some of the ways in which a PCI diagnostic can continue to support US objectives in stellarator physics research. Of the five areas identified in the FOA, the PCI diagnostic can make the strongest contributions to areas 2 and 3, with secondary contributions to areas 1 and 4.

Priority I: Understanding compatible core-edge solutions

The connection between properties of the edge plasma, where the plasma interfaces with the divertor units, and core performance is a critical area of research for achieving high performance

plasmas. The PCI diagnostic's ability to measure fluctuations across all flux surfaces means that it can simultaneously identify changes in the edge, such as the existence of coherent modes or a rise in turbulent fluctuations, and changes in core behavior that can be correlated with profile measurements. The addition of radial localization capability will further enhance the PCI diagnostic's ability to contribute to analysis of the relationship between core and edge performance.

Priority II: Understanding limits

The PCI diagnostic is ideally suited to assist with studies of the conditions and regimes of operation that offer improved energy and particle confinement. Comparisons of the magnitude and drift velocity associated with turbulent fluctuations under different magnetic configurations can lead to insights about the role of magnetic shear and the mirror ratio in determining what parameters of magnetic field design are most important to performance optimization. Additionally, the PCI diagnostic's sensitivity to density fluctuations induced by Alfvénic activity means that it can be used to identify the location and role of energetic ions in high performance operation scenarios. PCI will also show if high-β operation is compatible with the onset of electromagnetic kinetic ballooning modes which may limit further performance increases regardless of electrostatic mode stabilization.

Priority III: Exploiting U.S. hardware investments

High-density, core-fueled operation with the new Oak Ridge-PPPL pellet injector system will present many opportunities to study the relationship between fluctuations and confinement. Prior analyses with the PCI system have already focused on pellet-fueled plasmas, and have shown interesting transitions in behavior as higher-density operation is reached [4]. Prior analyses with the PCI system have already focused on transient turbulence suppression by core density peaking in pellet-fueled plasmas. PCI will demonstrate if this suppression mechanism can be extended into a viable steady-state operation scenario using the new continuous injector system.

Priority IV: Long-pulse, high power operation

While the measurements from the PCI system are typically more concerned with short-timescale fluctuations in the plasma, the ability to monitor changes in fluctuation spectra over longer periods (using a multi-window data acquisition setup) will allow the PCI diagnostic to contribute to studies of the role of bootstrap currents and high β effects on overall confinement. While the measurements from our PCI system are typically more concerned with short-timescale fluctuations in the plasma, PCI has the ability to non-invasively monitor changes in fluctuation spectra over longer periods by continuous streaming data acquisition. We can thereby contribute to studies of stationary detachment, heat-load induced divertor outgassing and bootstrap current evolution during long-timescale thermal equilibration of plasma-facing components.